Journal of Quantitative Spectroscopy & Radiative Transfer 208 (2018) 164–171

Contents lists available at ScienceDirect

Journal of Quantitative Spectroscopy & Radiative Transfer

journal homepage: www.elsevier.com/locate/jqsrt

Light transfer through windows with external condensation

Keyong Zhu[a], Shaoling Li[a], Laurent Pilon[b,*]

[a] Beihang University, School of Aeronautical Science and Engineering, No. 37, Xueyuan Road, Beijing 100191, China
[b] University of California, Los Angeles, Mechanical and Aerospace Engineering Department, 420 Westwood Plaza, Los Angeles CA 90095-1597, USA

ARTICLE INFO

Article history:
Received 26 November 2017
Revised 7 January 2018
Accepted 12 January 2018
Available online 16 January 2018

Keywords:
External condensation
Dew
Dropwise condensation
Energy efficient windows
Visibility reduction
Solar cell efficiency

ABSTRACT

This study investigates systematically light transfer through windows supporting cap-shaped droplets on their external face. The presence of such droplets may have negative effects on the conversion efficiency of solar cells, distorts image quality of lenses, or hinders visibility through windows and windshields. Here, the directional-hemispherical transmittance was predicted by the Monte Carlo ray-tracing method. The droplets were monodisperse or polydisperse randomly distributed on the outside face of optically smooth windows. For nonabsorbing droplets, the diameter and size distribution did not have a significant effect on the window directional-hemispherical transmittance. The latter was nearly independent of contact angle for incident angle $\theta_i \leq 30°$. However, the directional-hemispherical transmittance decreased monotonously with increasing incident angle and droplet contact angle for contact angle $\theta_c \leq 70°$ to reach a minimum at a contact angle $\theta_{c,min}$ beyond which it increased with increasing contact angle before reaching a plateau at large contact angles. This was attributed to total internal reflection at the back window/air and droplet/air interfaces. For absorbing droplets, the normal-hemispherical transmittance decreased significantly with increasing droplet contact angle, mean diameter, polydispersity, and projected surface area coverage due to strong absorption within the droplets. Moreover, the normal-hemispherical transmittance decreased with increasing contact angle for $\theta_c < 90°$ and remained constant and independent of the droplets' absorption index, mean diameter, and contact angle for $\theta_c \geq 90°$. Finally, Analytical expressions for the upper and lower bounds of the normal-hemispherical transmittance as a function of droplet contact angle, optical properties, and projected surface area coverage were derived.

1. Introduction

The presence of droplets on the outside face of a window is common occurrence in numerous circumstances. In such situations, droplets are undesirable as they hinder visibility. For example, outside condensation on windows can be observed (i) on poorly insulated windows in air-conditioned buildings under hot and humid climates [1,2] or (ii) on well-insulated windows – with U-value less than 1.2 W/m^2.K – on clear and humid nights when the window external surface temperature falls below the dew point [3-5]. Outside condensation reduces the visibility through the window and has been identified as a factor limiting adoption of more energy efficient windows [5]. Two types of surface coatings have been explored to reduce outside condensation on well-insulated windows namely (1) a low-emissivity coating (e.g., SnO_2:F) to reduce radiation cooling and increase the window outside surface temperature and (2) a hydrophilic coating (e.g., TiO_2) to ensure that condensed water forms a transparent water film instead of strongly scattering droplets [2,4].

Similarly, outside condensation on vehicle windshields and from water sprayed by other vehicles driving on wet roads can significantly reduce road visibility, particularly at night and despite the use of wipers [6]. Dropwise condensation also occurs on lenses of cameras used for scientific observations [7,8] and surveillance [9]. Finally, the presence of water droplets on photovoltaic solar cells from dew or rain could decrease the efficiency of solar cells due to light absorption and reflection by the water droplets [10,11].

The present paper aims to investigate systematically light transfer through windows supporting cap-shaped droplets on their outside face. The effects of incident angle and of droplet size distribution, contact angle, projected surface area coverage, and absorption index were investigated. The results will provide guidelines for the design and material selection of building and car windows, camera lenses, and solar cells in order to reduce the negative effects of droplets on window transmittance and system performance.

* Corresponding author.
E-mail address: pilon@seas.ucla.edu (L. Pilon).

https://doi.org/10.1016/j.jqsrt.2018.01.019
0022-4073/

Nomenclature

A_n	normal absorptance
d	droplet diameter, µm
d_m	mean diameter of droplets, µm
d_p	projected diameter of droplets on the window, µm
f_A	droplet projected surface area coverage
H	thickness of the window, mm
k	absorption index
L	length of the window, mm
M	number of photon bundles
n	refractive index
R	reflectance
T	transmittance
W	width of the window, mm

Greek symbols

θ_c	contact angle, °
θ_i	incident angle, °
λ	wavelength, µm
ρ_{ij}	reflectivity of the interface i/j
σ	standard deviation of droplet diameter, µm
τ	transmissivity

Subscripts

a	refers to air
d	refers to droplet
f	refers to film
w	refers to window
dh	refers to directional-hemispherical
nh	refers to normal-hemispherical

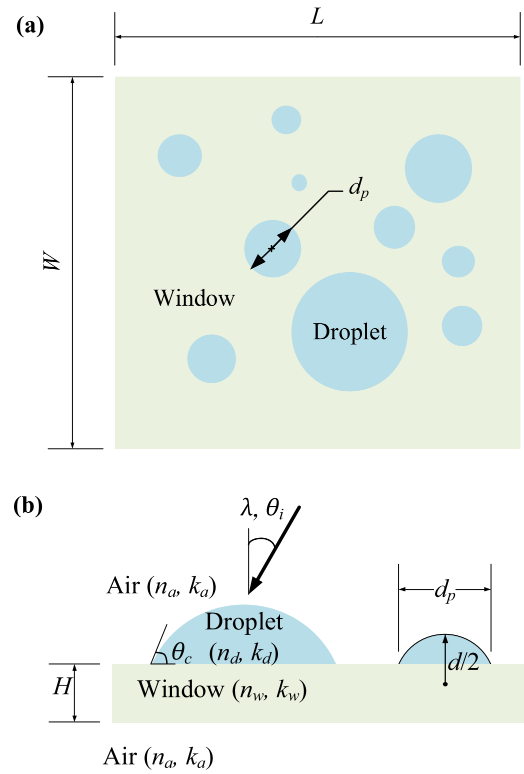

Fig. 1. (a) Top view of the semitransparent window (n_w, k_w) of dimensions $L \times W \times H$ supporting polydisperse absorbing cap-shaped droplets (n_d, k_d) for contact angle θ_c, diameter d, and projected diameter d_p. (b) Cross-section of the semitransparent window supporting absorbing droplets exposed to collimated incident radiation at angle θ_i and wavelength λ.

2. Analysis

2.1. Problem statement

Fig. 1(a) and 1(b) respectively show the top and side views of polydisperse droplets randomly distributed on the outside face of a window of length L, width W, and thickness H. Collimated monochromatic radiation of wavelength λ was incident on the outside face of the window at a polar angle θ_i. Photons were reflected, transmitted, or absorbed by the window with refractive and absorption indices, respectively denoted by n_w and k_w, or by the droplets with refractive and absorption indices denoted by n_d and k_d, respectively. In the present study, the dimensions of the window supporting randomly distributed monodisperse or polydisperse droplets were $L = W = 5$ mm, and $H = 3$ mm. Unless otherwise noticed, the refractive and absorption indices of the surrounding air were taken as $n_a = 1.0$ and $k_a = 0$, and the refractive indices of the window and droplets were taken as $n_w = 1.5$ and $n_d = 1.33$, respectively. The window and droplet absorption indices k_w and k_d were taken as parameters as they can vary strongly with wavelength. Finally, the projected surface area coverage f_A was defined as the fraction of the glass window covered by the normal projection of droplets with diameter d and contact angle θ_c whose projected diameter d_p can be expressed as

$$d_p = d \sin[\min(\theta_c, 90^\circ)]. \quad (1)$$

2.2. Methods

Monodisperse or polydisperse and randomly distributed droplets were generated on the outside face of the window by using the same methodology as that developed in our previous study focused on light transfer through windows supporting droplets on their back side [12,13]. The procedure was described in detail in Ref. [12] and need not be repeated. Similarly, simulations of light transfer through windows supporting droplets on their outside face was based on the same assumptions as that used in Ref. [12,13] in order to make the problem mathematically tractable. In brief, all interfaces were assumed to be optically smooth and Snell's law and Fresnel's equations prevailed. Here also, Monte Carlo ray-tracing method [14,15] was used to predict the directional-hemispherical reflectance, transmittance, and absorptance of windows exposed to collimated radiation and supporting droplets on their outside face [12,13]. In all simulations reported in this paper, the total number of photon bundles simulated was $M = 10^6$ in order to achieve numerical convergence.

3. Results and discussion

A parametric study was performed to investigate systematically the effects of (i) incident angle θ_i, (ii) normal droplet size distribution, (iii) contact angle θ_c, (iv) projected surface area coverage f_A, and (v) droplet absorption index k_d on the normal-hemispherical transmittance and reflectance of semitransparent windows supporting either nonabsorbing ($k_d = 0$) or absorbing ($k_d > 0$) droplets.

3.1. Nonabsorbing droplets on transparent window

3.1.1. Effect of droplet diameter and size distribution

Fig. 2 shows the directional-hemispherical transmittance for nonabsorbing ($k_d = 0$) droplets and transparent ($k_w = 0$) window (a) as a function of incident angle θ_i for contact angle $\theta_c = 60°$ and $\theta_c = 120°$, and (b) as a function of contact angle θ_c with incident angle $\theta_i = 30°$ and $\theta_i = 60°$. Fig. 2 compares predictions

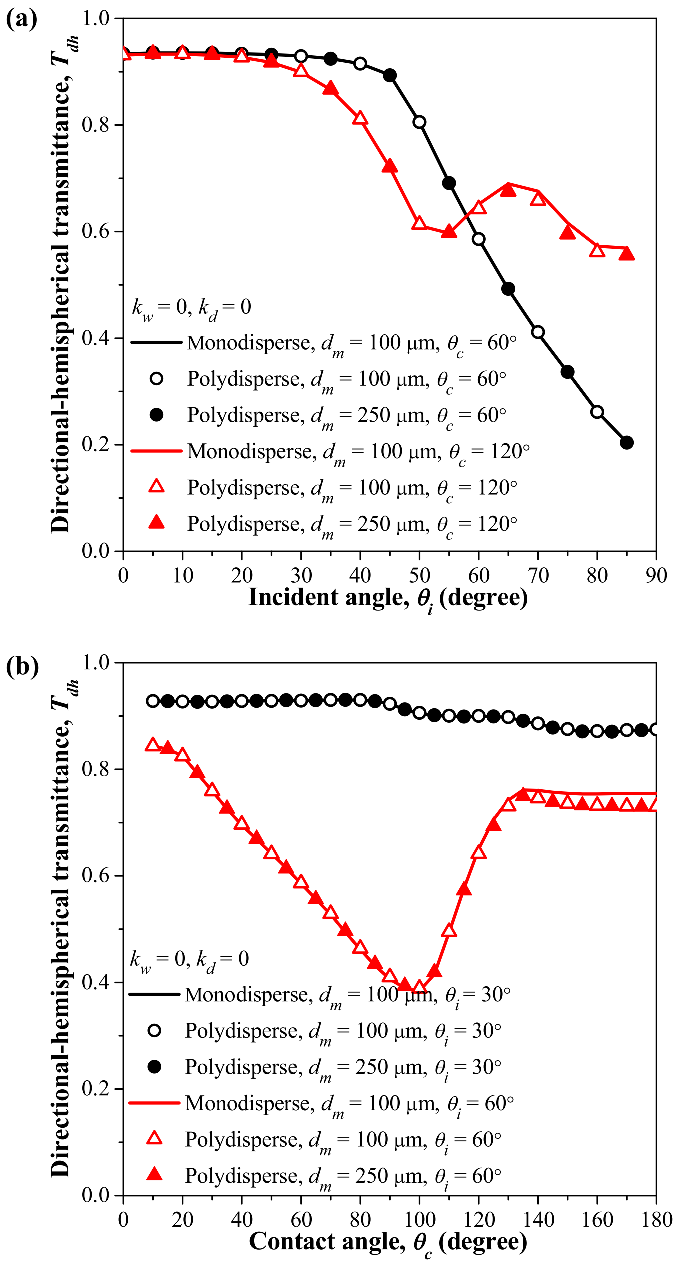

Fig. 2. Directional-hemispherical transmittance for nonabsorbing droplets on transparent windows (a) as a function of incident angle θ_i for contact angle $\theta_c = 60°$ and $\theta_c = 120°$, and (b) as a function of contact angle θ_c for incident angle $\theta_i = 30°$ and $\theta_i = 60°$. The monodisperse or polydisperse droplets were randomly distributed with either $d_m = 100$ μm or $d_m = 250$ μm. The diameter of polydisperse droplets was $d_m - \sigma < d < d_m + \sigma$ and such that $\sigma = d_m$. Here, $f_A = 50\%$, $n_w = 1.5$, and $n_d = 1.33$.

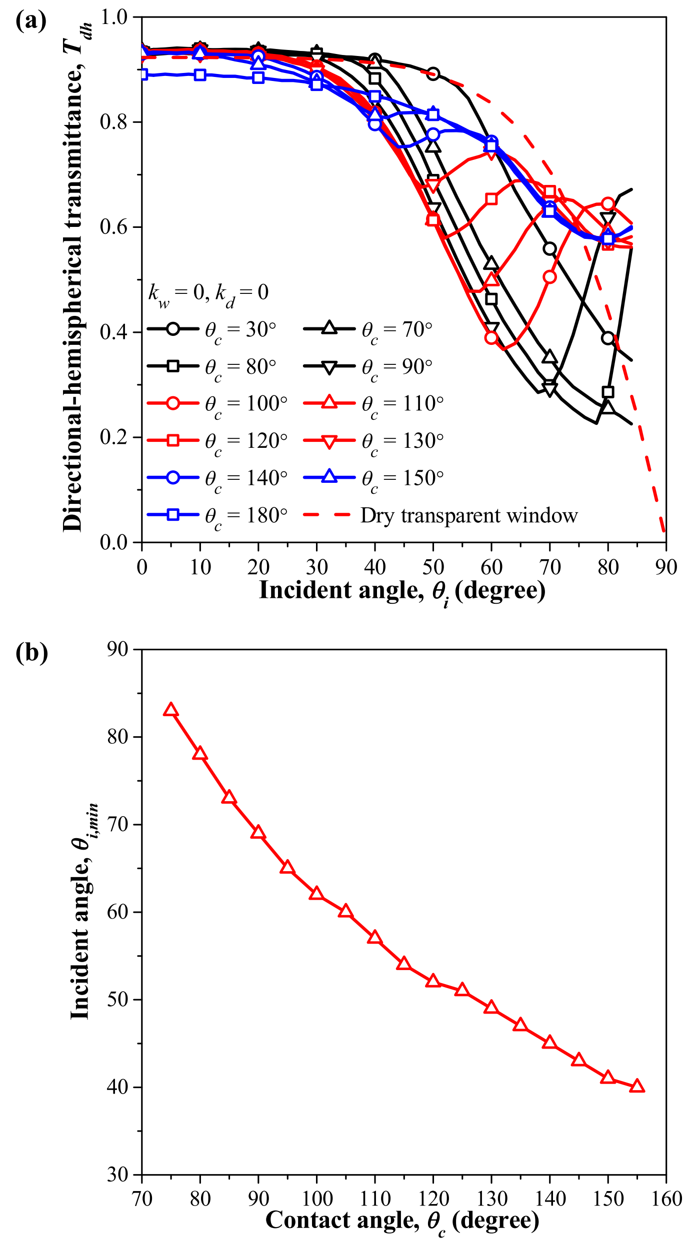

Fig. 3. (a) Directional-hemispherical transmittance for nonabsorbing droplets on transparent windows as a function of incident angle θ_i for different values of contact angle θ_c and (b) incident angle $\theta_{i,min}$ corresponding to the minimum transmittance as a function of contact angle θ_c. The droplets were monodisperse and randomly distributed with $d_m = 250$ μm, $f_A = 50\%$, $n_w = 1.5$, and $n_d = 1.33$.

for randomly distributed (i) monodisperse and (ii) polydisperse droplets following a normal distribution with mean diameter d_m and standard deviation σ with droplet diameter such that $d_m - \sigma < d < d_m + \sigma$. The droplet mean diameter was either $d_m = 100$ μm or 250 μm while standard deviation of polydisperse droplets was $\sigma = d_m$ and the droplet projected surface area coverage was $f_A = 50\%$. Fig. 2 indicates that, for nonabsorbing droplets, the droplet mean diameter and their size distribution had a negligibly small effect on the directional-hemispherical transmittance. Similar observations were made for transparent windows with nonabsorbing droplets on their backside [12]. These results simplify the analysis by reducing the directional-hemispherical transmittance to a function such that $T_{dh} = T_{dh}$ (n_w, n_d, θ_i, θ_c, f_A).

Finally, it is important to note that the presence of droplets on the external surface of the window leads to very different photon optical path and transmittance compared with droplets on the backside, as illustrated in Supplementary Material for transparent window and non-absorbing droplets for a wide range of contact angle and incident directions.

3.1.2. Effect of incident angle

Fig. 3 plots (a) the directional-hemispherical transmittance for monodisperse and randomly distributed nonabsorbing droplets and transparent window as a function of incident angle θ_i for different contact angle θ_c and (b) the incident angle $\theta_{i,min}$ corresponding to the minimum transmittance as a function of contact angle θ_c. Here, the droplet diameter was $d_m = 250$ μm and the droplet projected surface area coverage was $f_A = 50\%$. Fig. 3(a) indicates that, for incident angle $\theta_i \leq 40°$ and all contact angles considered, the directional-hemispherical transmittance remained nearly constant and identical to that of the dry transparent window. Then, it decreased monotonously with increasing incident angle for contact angle $\theta_c < 70°$. However, for contact angle $\theta_c \geq 70°$, the directional-hemispherical transmittance featured a minimum at the incident angle $\theta_{i,min}$. Fig. 3(b) indicates that the incident angle $\theta_{i,min}$ decreased with increasing contact angle $\theta_c \geq 70°$. The presence of a minimum in the directional-hemispherical transmittance could be attributed to total internal reflection at the back window/air and droplet/air interfaces. However, simple expressions relating $\theta_{i,min}$ to θ_c could not be formulated due to the complexity of the optical path. Indeed, photons entering the window either directly or through the droplets may get internally reflected at the back window/air interface ($n_w > n_a = 1$) and enter the droplets followed by internal reflection at the droplet/air interface ($n_d > 1$).

In order to prove the effect of total internal reflection at the back window/air and droplet/air interfaces, Fig. 4 shows the directional-hemispherical transmittance T_{dh} for transparent window supporting nonabsorbing monodisperse droplets as a function of incident angle θ_i (a) for different values of refractive indices of the window n_w (= 1.5 or 1.33) and the droplets n_d (= 1.33 or 1.5) while keeping $n_a = 1$, and (b) for the imaginary cases when the inside and outside air is replaced by media with respective refractive indices $n_{a,i}$ and $n_{a,o}$ (= 1 or 1.5) while keeping $n_w = 1.5$ and $n_d = 1.33$. Here also, the droplet diameter was $d_m = 250$ µm, contact angle was $\theta_c = 90°$, and the droplet projected surface area coverage was $f_A = 50\%$. Fig. 4(a) indicates that, for a given droplet refractive index n_d, the window refractive index n_w had a negligible effect on the directional-hemispherical transmittance T_{dh} and thus on the incident angle $\theta_{i,min}$. In other words, suppressing reflection and refraction at the droplet/window interface by matching their refractive indices had a negligible effect. By contrast, for a given value of n_w, increasing the droplets refractive index n_d and thus the refractive index mismatch between the droplet and the air resulted in increasing the incident angle $\theta_{i,min}$. Moreover, Fig. 4(b) indicates that, for $n_{a,o} = 1.5$ and $n_{a,i} = 1$, the directional-hemispherical transmittance T_{dh} decreased sharply around 42° corresponding to the critical angle for total internal reflection at the back window/air interface given by $\theta_{i,cr} = \sin^{-1}(n_{a,i}/n_w) \approx 41.8°$. In addition, T_{dh} further decreased beyond $\theta_{i,cr}$ to vanish for incident angles above the cut-off incident angle $\theta_{i,co} \approx 54.2°$ expressed, according to successive applications of Snell's law, as $\theta_{i,co} = \cos^{-1}\left(\sqrt{n_d^2 - n_{a,i}^2}/n_{a,o}\right)$. For $n_{a,o} = 1$ and $n_{a,i} = 1.5$, T_{dh} remained constant and almost independent of incident angle. This could be attributed to the absence of reflection on the back face of the glass window. For $n_{a,o} = 1.5$ and $n_{a,i} = 1.5$, T_{dh} decreased rapidly at large incident angle. These results confirm that total internal reflection at the back window/air and air/droplet interfaces was responsible for the behavior of T_{dh} (Fig. 3(a)) and the existence of the incident angle $\theta_{i,min}$ (Fig. 3(b)) which depended on contact angle θ_c.

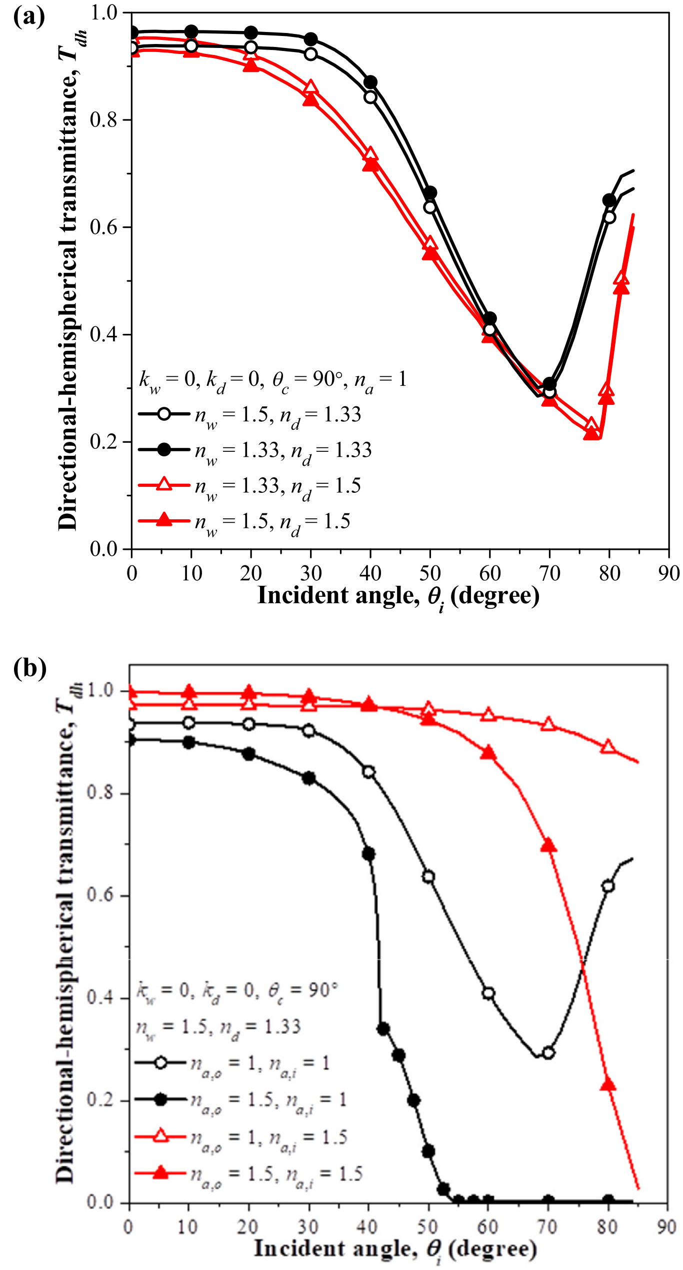

Fig. 4. Directional-hemispherical transmittance for nonabsorbing droplets on transparent windows as a function of incident angle θ_i with (a) different refractive indices of windows and droplets, n_w and n_d, and (b) different refractive indices of air above the window on the droplet side and air below the window backside, $n_{a,t}$ and $n_{a,b}$. The droplets were monodisperse and randomly distributed with $d_m = 250$ µm, $\theta_c = 90°$, $f_A = 50\%$.

3.1.3. Effect of droplet contact angle

Fig. 5 shows the directional-hemispherical transmittance for transparent window supporting nonabsorbing monodisperse droplets as a function of contact angle θ_c with different incident angle θ_i. Here also, the droplet diameter was $d_m = 250$ µm and the droplet projected surface area coverage was taken as $f_A = 50\%$. Fig. 5 indicates that the hemispherical transmittance for incident angle θ_i less than 30° was nearly independent of contact angle θ_c except for a slight decrease for contact angles $\theta_c > 160°$. However, the directional-hemispherical transmittance for large incident angle $\theta_i \geq 40°$ decreased with increasing contact angle to reach a minimum at a contact angle $\theta_{c,min}$. Beyond $\theta_{c,min}$, the directional-hemispherical transmittance increased with increasing contact angle before reaching a plateau at large contact angles. The contact angle $\theta_{c,min}$ decreased with increasing incident angle θ_i, as illustrated in the previously discussed Fig. 3(b). Again, this was attributed to total internal reflection at the back window/air and droplet/air interfaces.

3.1.4. Effect of projected surface area coverage

Fig. 6 plots the normal-hemispherical transmittance T_{nh} of transparent windows supporting nonabsorbing droplets with contact angle θ_c between 0 and 180° for different values of projected surface area coverage $f_A = 10\%$, 30%, and 50%. The droplet diameter was $d_m = 250$ µm. Fig. 6 also shows the normal transmittance for a nonabsorbing window without and with a nonabsorbing

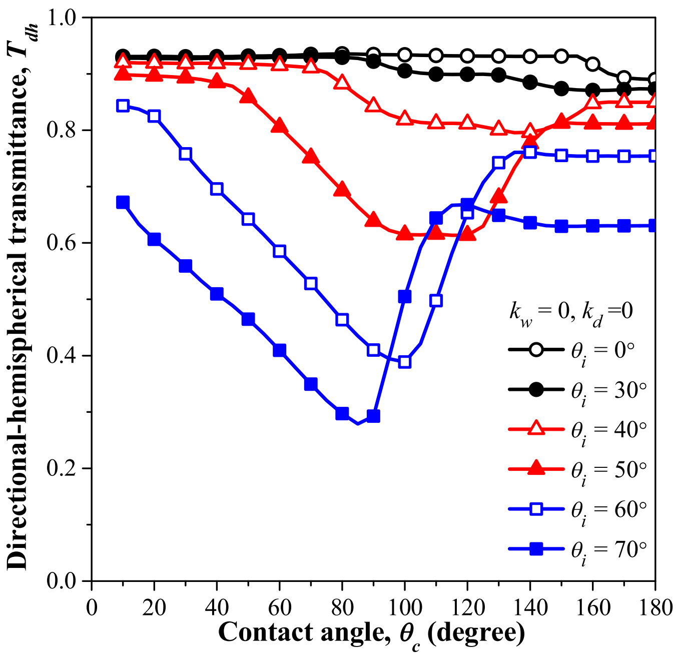

Fig. 5. Directional-hemispherical transmittance for nonabsorbing droplets on transparent windows as a function of contact angle θ_c for different incident angle θ_i. The droplets were monodisperse and randomly distributed with $d_m = 250$ µm, $f_A = 50\%$, $n_w = 1.5$, and $n_d = 1.33$.

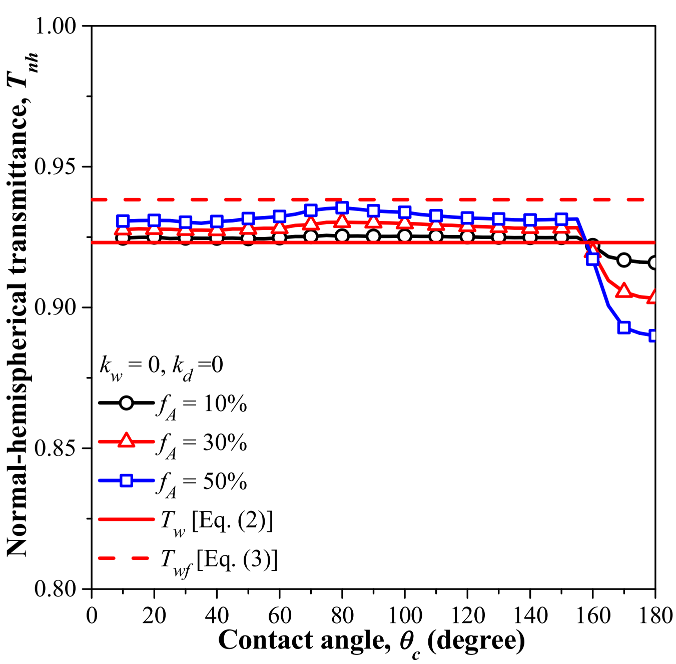

Fig. 6. Normal-hemispherical transmittance for nonabsorbing droplets on transparent windows for different projected surface area coverage f_A. The droplets were monodisperse and randomly distributed with $d_m = 250$ µm, $n_w = 1.5$, and $n_d = 1.33$.

liquid film of thickness identical to the average height of cap-shaped droplets given by $H_f = (1 - \cos\theta_c)d_m/2$. The normal-normal transmittance T_w of the dry transparent window ($k_w = 0$) can be expressed as [14]

$$T_w = (1 - \rho_{aw})/(1 + \rho_{aw}), \tag{2}$$

where ρ_{aw} is the reflectivity of the air/window interface expressed as $\rho_{aw} = (n_a - n_w)^2/(n_a + n_w)^2$.

Similarly, the normal-normal transmittance T_{wf} of the transparent window covered with a nonabsorbing film can be written as [14]

$$T_{wf} = \frac{\left(1 - \rho_{af}\right)\left(1 - \rho_{fw}\right)(1 - \rho_{wa})}{\left(1 - \rho_{af}\rho_{fw}\right)\left(1 - \rho_{fw}\rho_{wa}\right) - \rho_{af}\rho_{wa}\left(1 - \rho_{fw}\right)^2}, \tag{3}$$

where ρ_{af}, ρ_{fw}, and ρ_{wa} are respectively the specular normal reflectivities at the air/film, film/window, and window/air interfaces and given by $\rho_{ij} = (n_i - n_j)^2/(n_i + n_j)^2$.

Fig. 6 indicates that, for contact angles $\theta_c < 160°$, the normal-hemispherical transmittance of the window with nonabsorbing droplets was independent of θ_c, as previously discussed. In addition, it increased slightly with increasing projected surface area coverage f_A. It is also interesting to note that the normal-hemispherical transmittance was larger than the transmittance of dry transparent window T_w and smaller that of the window with a nonabsorbing film T_{wf} for $\theta_c < 160°$. This can be attributed to the reduction in reflection thanks to the smaller index mismatch achieved by the presence of the droplets compared with the dry window. However, for contact angle $\theta_c > 160°$, the presence of the droplets reduced the normal-hemispherical transmittance of the window. This effect was stronger with increasing projected surface area coverage f_A. This could be attributed to the lack of total internal reflection in the droplets for large contact angles and the resulting increase in reflectance.

3.2. Absorbing droplets on transparent windows

3.2.1. Effects of size distribution and droplet diameter

Fig. 7 shows (a) the normal-hemispherical transmittance T_{nh} and (b) the normal absorptance A_n of transparent windows ($k_w = 0$) supporting monodisperse or polydisperse absorbing droplets ($k_d = 10^{-3}$) at wavelength $\lambda = 1$ µm as a function of contact angle θ_c for different values of mean diameter d_m namely 100 µm and 250 µm. Note that in the case of absorbing droplets or windows, the wavelength needs to be specified to estimate their absorption coefficient [13]. The droplets were randomly distributed on the window surface with projected surface area coverage $f_A = 50\%$ and had the same mean diameter d_m albeit the diameter of polydisperse droplets followed a normal distribution with $d_m - \sigma < d < d_m + \sigma$ and such that $\sigma = d_m$. Fig. 7(a) indicates that the normal-hemispherical transmittance decreased significantly and monotonously with increasing contact angle θ_c for both monodisperse and polydisperse droplets. Unlike in the case of nonabsorbing droplets, the mean diameter d_m and size distribution of absorbing droplets affected the normal-hemispherical transmittance T_{nh}. In fact, the latter decreased and the normal absorptance A_n increased as the droplet diameter and/or polydispersity increased. This was due to the fact that, the volume of the droplets – and the fraction of incident radiation they absorbed – increased with increasing droplet contact angle θ_c and/or mean diameter d_m, as illustrated in Fig. 7(b). Finally, the normal-hemispherical reflectance was small ($< 7\%$), and decreased slightly with increasing contact angles.

3.2.2. Effect of droplet absorption index k_d

Fig. 8 plots the normal-hemispherical transmittance T_{nh} of a transparent window supporting, on its outside face, monodisperse absorbing droplets with different values of absorption indices k_d. The droplets were randomly distributed with diameter (a) $d_m = 100$ µm or (b) $d_m = 250$ µm, and projected surface area coverage $f_A = 50\%$. Fig. 8 indicates that the normal-hemispherical transmittance decreased slightly with increasing contact angle for slightly absorbing droplets ($k_w = 0$ and $k_d = 10^{-4}$). However, for

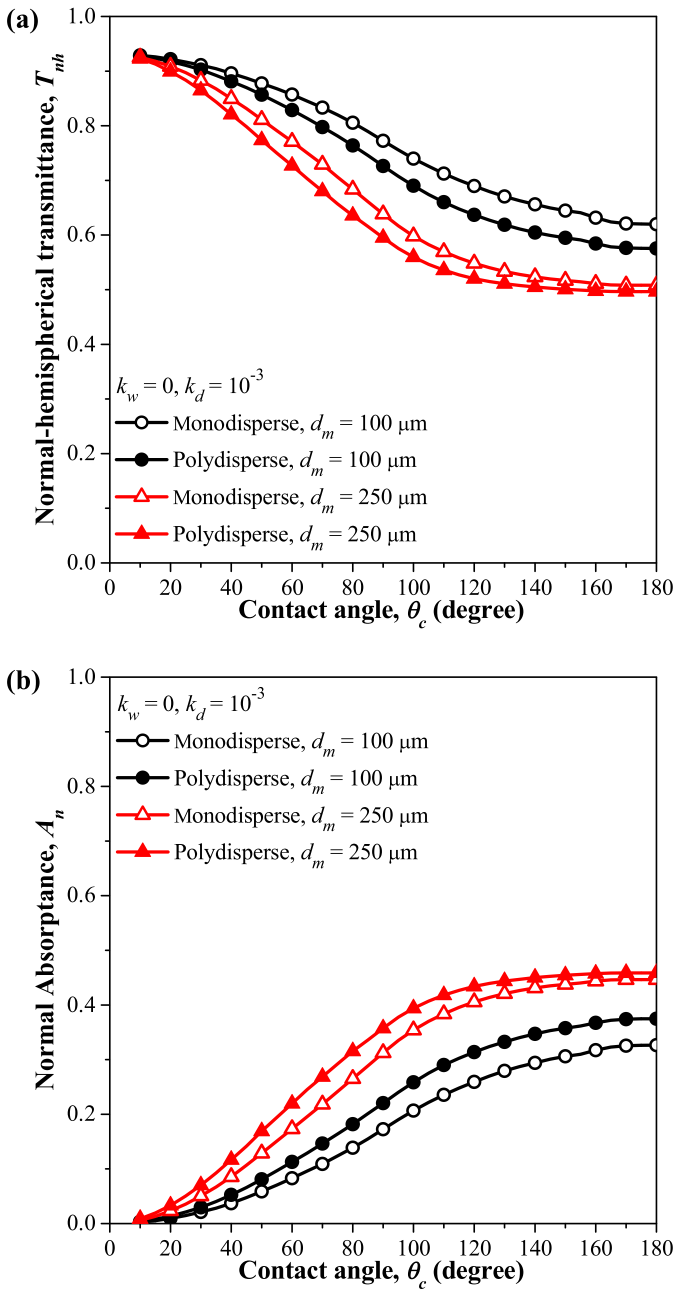

Fig. 7. (a) Normal-hemispherical transmittance ($\theta_i = 0°$) and (b) normal absorptance of transparent windows ($k_w = 0$) supporting monodisperse or polydisperse absorbing droplets ($k_d = 10^{-3}$) as a function of contact angle θ_c for droplet mean diameter d_m of 100 and 250 μm. The droplets were randomly distributed with $f_A = 50\%$, $\lambda = 1$ μm, $n_w = 1.5$, and $n_d = 1.33$. The diameter of polydisperse droplets followed a normal distribution with $d_m - \sigma < d < d_m + \sigma$ and such that $\sigma = d_m$.

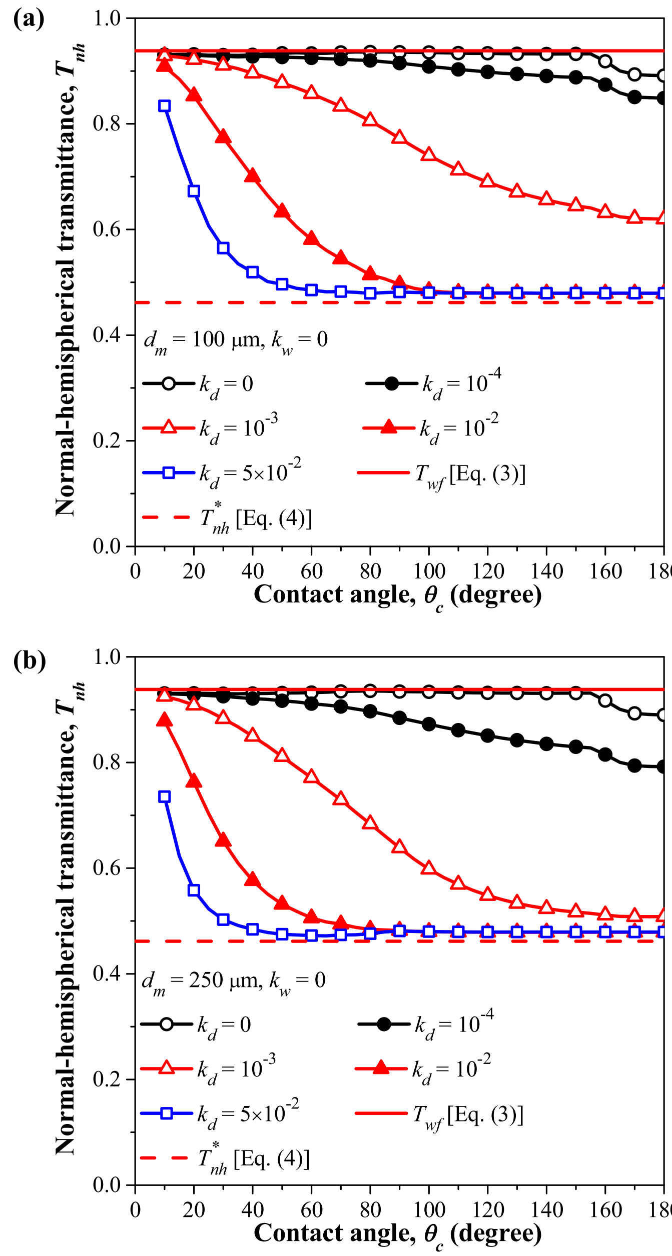

Fig. 8. Normal-hemispherical transmittance for absorbing droplets on transparent windows with different absorption index k_d. The droplets were monodisperse and randomly distributed with (a) $d_m = 100$ μm or (b) $d_m = 250$ μm with $f_A = 50\%$, $\lambda = 1$ μm, $n_w = 1.5$, and $n_d = 1.33$.

strongly absorbing droplets ($k_w = 0$ and $k_d \geq 10^{-2}$), the normal-hemispherical transmittance T_{nh} decreased significantly with increasing contact angle for $\theta_c < 90°$ The decrease was sharper for larger droplets for a given value of k_d. On the other hand, for $\theta_c \geq 90°$, T_{nh} remained constant and independent of (i) absorption index k_d, (ii) droplet mean diameter d_m, and (iii) contact angle θ_c. This could be attributed to the fact that, for $k_d \geq 10^{-2}$, all photons entering the droplets were absorbed. In fact, for $\theta_c \geq 90°$, the normal-hemispherical transmittance corresponded to the fraction of radiation directly entering the dry areas of the front window and could be expressed approximately as

$$T_{nh}^* \approx T_w(1 - f_A), \tag{4}$$

where T_w is the normal-normal transmittance of the dry transparent window given by Eq. (2). These conclusions were similar to those obtained in the case of windows supporting absorbing droplets on their backside [13]. Fig. 8 also plots the normal-hemispherical transmittance T_{wf} of a transparent window covered with a nonabsorbing film ($n_d = 1.33$, $k_d = 0$) of thickness H_f = (1-cosθ_c)d_m/2 given by Eq. (3). It indicates that the normal-hemispherical transmittance of transparent windows covered with absorbing droplets fell between T_{wf} and T_{nh}^* predicted by Eqs. (3) and (4), respectively.

3.2.3. Effect of projected surface area coverage f_A

Fig. 9 plots the normal-hemispherical transmittance for transparent windows ($n_d = 1.5$, $k_d = 0$) supporting monodisperse and absorbing droplets ($n_d = 1.33$, $k_d = 10^{-3}$) of diameter $d_m = 250$ μm for different projected surface area coverage f_A. For $f_A = 0.1$, 0.3,

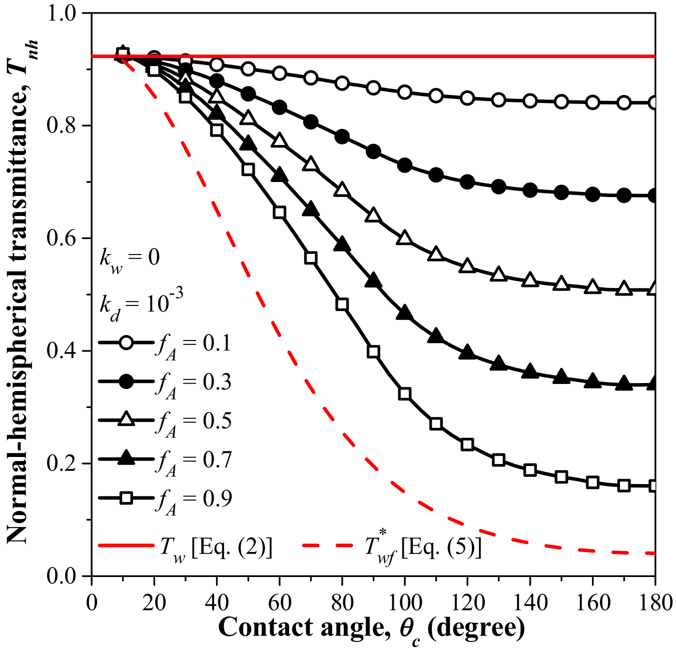

Fig. 9. Normal-hemispherical transmittance for absorbing droplets on transparent windows with different projected surface area coverage f_A. The droplets were monodisperse with $d_m = 250\,\mu$m, $\lambda = 1\,\mu$m, $n_w = 1.5$, and $n_d = 1.33$. For $f_A = 0.1$, 0.3, and 0.5, the droplets were randomly distributed and for $f_A = 0.7$ and 0.9, the droplets were arranged in an ordered hexagonal pattern.

and 0.5, the droplets were monodisperse randomly distributed and for $f_A = 0.7$ and 0.9, the droplets were arranged in an ordered hexagonal pattern. Indeed, it was difficult to achieve f_A above 0.5 with randomly distributed droplets. Fig. 9 also shows (i) the normal transmittance T_w for nonabsorbing dry window given by Eq. (2) and (ii) the normal-normal transmittance T^*_{wf} of the transparent window covered with an absorbing film of thickness $H_f = (1\text{-}\cos\theta_c)d_m/2$ and optical properties identical to those of the droplets expressed as [14]

$$T^*_{wf} = \frac{\left(1-\rho^*_{af}\right)\left(1-\rho^*_{fw}\right)\left(1-\rho^*_{wa}\right)\tau_f}{\left(1-\rho^*_{af}\rho^*_{fw}\tau_f^2\right)\left(1-\rho^*_{fw}\rho^*_{wa}\right)-\rho^*_{af}\rho^*_{wa}\,\tau_f^2\left(1-\rho^*_{fw}\right)^2}, \tag{5}$$

where $\tau_f = \exp(-4\pi k_f H_f/\lambda)$ is the normal transmissivity of the absorbing film while ρ^*_{af}, ρ^*_{fw}, and ρ^*_{wa} are the specular normal reflectivity at the air/film, film/window, and window/air interfaces respectively given by [14]

$$\rho^*_{ij} = \frac{\left(n_i - n_j\right)^2 + \left(k_i - k_j\right)^2}{\left(n_i + n_j\right)^2 + \left(k_i + k_j\right)^2}. \tag{6}$$

Fig. 9 indicates that the normal-hemispherical transmittance T_{nh} for absorbing droplets on transparent windows was smaller than the normal transmittance T_w for dry transparent window and larger than T^*_{wf} for transparent windows with an absorbing film with refractive and absorption indices n_d and k_d. The normal-hemispherical transmittance decreased with increasing projected surface area coverage f_A. This was due to the fact that larger projected surface area coverage f_A and contact angle θ_c resulted in larger droplets and stronger absorption of the incident radiation.

3.3. Absorbing droplets and semitransparent windows

Fig. 10 shows (a) the normal-hemispherical transmittance and (b) the associated normal absorptance for absorbing droplets

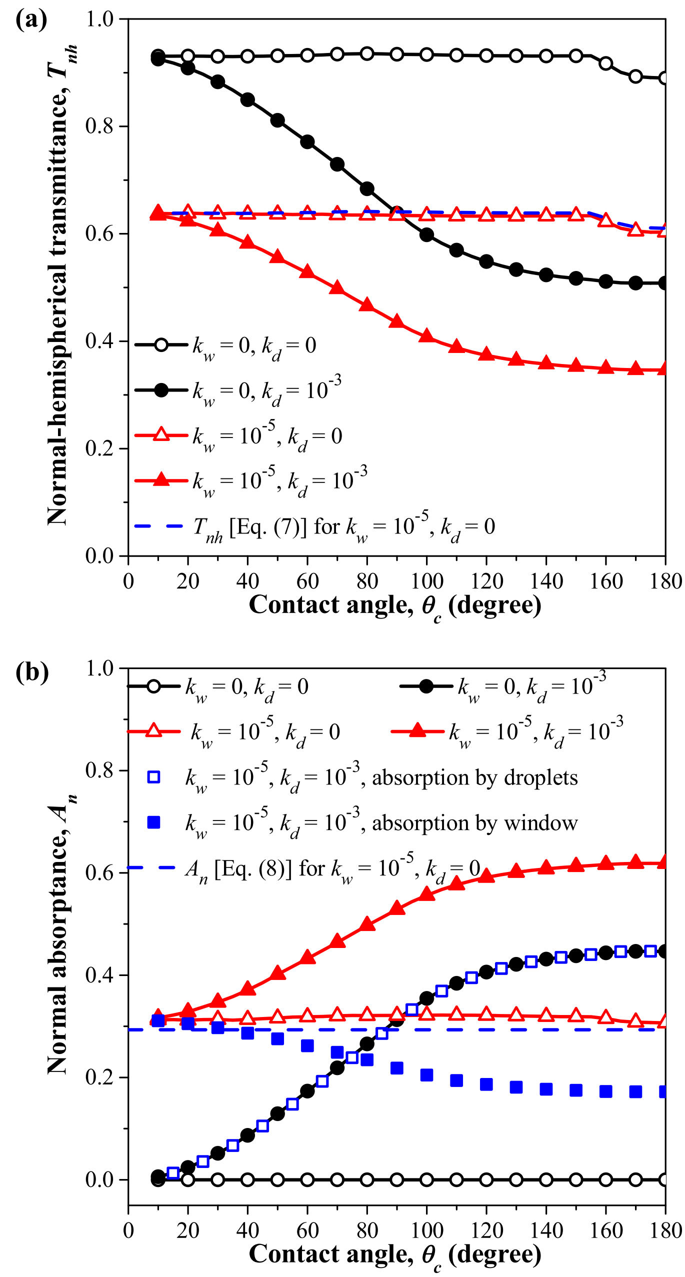

Fig. 10. (a) Normal-hemispherical transmittance and (b) normal absorptance for absorbing droplets on semitransparent windows with different values of k_w and k_d. The individual contributions of the droplets and window to the overall normal absorption are also shown. The droplets were monodisperse with $d_m = 250\,\mu$m, $f_A = 50\%$, $\lambda = 1\,\mu$m, $n_w = 1.5$ and $n_d = 1.33$.

($n_d = 1.33$) on semitransparent windows ($n_w = 1.5$) with different values of k_w and k_d. Fig. 10(b) also plots the individual contributions of the droplets and the window to the overall absorption. The droplets were monodisperse with $d_m = 250\,\mu$m and projected surface area coverage was $f_A = 50\%$. Fig. 10 indicates that, for nonabsorbing droplets ($k_d = 0$), the transmittance T_{nh} and absorbance A_n were nearly independent of contact angle θ_c, as previously discussed. However, for absorbing windows, the transmittance T_{nh} decreased with increasing window absorption index k_w according to

$$T_{nh}(k_w, k_d = 0, \theta_c) \approx T_{nh}(k_w = 0, k_d = 0, \theta_c)\tau_w, \tag{7}$$

where $\tau_w = \exp(-4\pi k_w H/\lambda)$ is the normal transmissivity of the window of thickness H ignoring reflectance at the interfaces. Similarly, despite the presence of nonabsorbing droplets, the normal absorptance A_n of the wet window was nearly equal to that of the dry window expressed as [14]

$$A_n(k_w, k_d = 0, \theta_c) \approx (1 - \rho^*_{aw})(1 - \tau_w)/(1 - \rho^*_{aw}\tau_w), \quad (8)$$

Then, based on energy conservation principles, the normal-hemispherical reflectance R_{nh} can be expressed as

$$R_{nh}(k_w, k_d = 0, \theta_c) = 1 - T_{nh} - A_n. \quad (9)$$

Fig. 10 also establishes that the normal-hemispherical transmittance T_{nh} and the normal absorptance A_n obtained from Monte Carlo simulations for $k_w = 10^{-5}$ and $k_d = 0$ were in excellent agreement with predictions by Eqs. (7) and (8), respectively.

Moreover, the normal-hemispherical transmittance T_{nh} for semitransparent window and absorbing droplets ($k_w = 10^{-5}$ and $k_d = 10^{-3}$) decreased monotonously with increasing contact angle θ_c while the corresponding normal absorptance A_n increased. In addition, the contribution of the window to the total absorption decreased with increasing contact angle θ_c while that of the droplets increased. This can be attributed to the increasing volume of droplets with increasing contact angle and the resulting absorption. In addition, the contribution of the droplets to the total absorption was almost identical to that when the window was transparent ($k_w = 0$ and $k_d = 10^{-3}$). Moreover, despite the relatively large surface coverage f_A, the droplets did not contribute significantly to the overall absorption for small contact angle $\theta_c < 50°$. Simultaneously, the contribution of the window to the total absorption decreased with increasing contact angle. This was due to the fact that, radiation was first absorbed by the droplets and then by the window. Thus, with increasingly large droplets, less radiation entered the window and less could be absorbed.

These results can be used to estimate the efficiency of solar cells covered with droplets. As a first order approximation, the latter is equal to the product of the solar cell efficiency without droplets and the normal-hemispherical transmittance reported in the present study. In the case of external condensation reducing the visibility through windows, a more detailed study should be performed as droplets not only reduce the intensity of the transmitted light but also modify its direction, thus distorting the image of the object considered.

4. Conclusion

This study investigated the directional-hemispherical transmittance of windows supporting cap-shaped droplets on their outside face exposed to incident collimated light. The droplets were monodisperse or polydisperse and randomly distributed on the window surface. The Monte Carlo ray-tracing method was used to predict the directional-hemispherical transmittance and reflectance of wet windows for a wide range of droplet diameter, contact angle, absorption index, projected surface area coverage, and window absorption index. First, for nonabsorbing droplets, the directional-hemispherical transmittance was independent of droplet diameter and size distribution. For incident angle $\theta_i \le 30°$, contact angle θ_c had a negligible effect on the directional-hemispherical transmittance. For large incident angle $\theta_i \ge 40°$, the transmittance decreased with increasing contact angle to reach a minimum at a contact angle $\theta_{c,min}$ beyond which it increased with increasing contact angle before reaching a plateau for large contact angles. In addition, the normal-hemispherical transmittance increased slightly with increasing projected surface area coverage for almost all contact angles.

By contrast, for absorbing droplets, the normal-hemispherical transmittance decreased significantly with increasing droplet diameter, contact angle, polydispersity, and projected surface area coverage due to the associated increase in the total droplet volume. The normal-hemispherical transmittance of wet window decreased with increasing contact angle for $\theta_c < 90°$ and remained constant and independent of the droplets' absorption index, mean diameter, and contact angle for $\theta_c \ge 90°$. Analytical expressions for the upper and lower bounds of the normal-hemispherical transmittance were also derived. These results can be used to select the material and surface coating to increase the conversion efficiency of solar cells and improve the visibility of windshield of transportation vehicles and building windows as well as the image quality of cameras.

Acknowledgments

This study was supported in part by the National Natural Science Foundation of China (No. 51406006) and the U.S. Advanced Research Project Agency–Energy (DE-AR0000738).

Supplementary materials

Supplementary material associated with this article can be found, in the online version, at doi:10.1016/j.jqsrt.2018.01.019.

References

[1] El Diasty R, Budaiwi I. External condensation on windows. Constr Build Mater 1989;3:135–9.
[2] Werner A, Roos A. Condensation tests on glass samples for energy efficient windows. Sol Energy Mater Sol Cells 2007;91:609–15.
[3] Werner A, Roos A, Nilsson P. Design and evaluation of a detection system for external water condensation on low U-value windows. Sens Actuators A 2007;138:16–21.
[4] Werner A, Roos A. Simulations of coatings to avoid external condensation on low U-value windows. Opt Mater 2008;30:968–78.
[5] Nair G, Mahapatra K, Gustavsson L. Implementation of energy-efficient windows in Swedish single-family houses. Appl Energy 2012;89:329–38.
[6] Hautière N, Dumont E, Brémond R, Ledoux V. Review of the mechanisms of visibility reduction by rain and wet road. In: International symposium on automotive lighting. Darmstadt, Germany; 2009. p. 445–55.
[7] Carthew SM, Slater E. Monitoring animal activity with automated photography. J Wildl Manage 1991;55:689–92.
[8] Probst RG, Gaughan N, Abraham M, Andrew J, Daly P, Hileman E, et al. Program status of NEWFIRM, the wide-field infrared camera system for the NOAO 4-m telescopes. In: Proceedings of SPIE. Bellingham, United States; 2004. p. 1716–1724.
[9] Kondou M. Condensation prevention camera device. United States Patent; 2016. No. 9525809.
[10] Panjwani MK, Narejo GB. Effect of humidity on the efficiency of solar cell (photovoltaic). Int J Eng Res General Sci 2014;2:499.
[11] Mekhilef S, Saidur R, Kamalisarvestani M. Effect of dust, humidity and air velocity on efficiency of photovoltaic cells. Renewable Sustainable Energy Rev 2012;16:2920–5.
[12] Zhu K, Huang Y, Pruvost J, Legrand J, Pilon L. Transmittance of transparent windows with nonabsorbing cap-shaped droplets condensed on their backside. J Quant Spectrosc Radiat Transfer 2017;194:98–107.
[13] Zhu K, Pilon L. Transmittance of semitransparent windows with absorbing cap-shaped droplets condensed on their backside. J Quant Spectrosc Radiat Transfer 2017;201:53–63.
[14] Howell JR, Siegel R, Mengüç MP. Thermal radiation heat transfer. fifth ed. Boca Raton: CRC Press; 2015.
[15] Modest MF. Radiative heat transfer. San Diego, CA: Academic Press; 2003.